Journal of Catalysis 282 (2011) 47–53

Contents lists available at ScienceDirect

Journal of Catalysis

journal homepage: www.elsevier.com/locate/jcat

Exploring the void structure and activity of RUB-39 based expanded materials using the hydroconversion of decane

Bart Tijsebaert [a], Mathieu Henry [a], Hermann Gies [b], Feng-Shou Xiao [c], Weiping Zhang [d], Xinhe Bao [d], Hiroyuki Imai [e], Takashi Tatsumi [e], Ulrich Müller [f], Bilge Yilmaz [f], Pierre Jacobs [a], Dirk De Vos [a,*]

[a] Centre for Surface Chemistry and Catalysis, K.U.Leuven, Kasteelpark Arenberg 23, 3001 Leuven, Belgium
[b] Ruhr-Universität Bochum, Institut für Geologie, Mineralogie und Geophysik, Universitätsstraße 150, NA 03/588, 44780 Bochum, Germany
[c] Department of Chemistry, Zhejiang University, Hangzhou 310028, China
[d] Dalian Institute for Chemical Physics, State Key Laboratory Catalysis, Dalian 116023, China
[e] Tokyo Institute of Technology, Nagatsuta 4259, Midori-ku, Yokohama 226-8503, Japan
[f] BASF, GCC/Z M 301, Chemicals Research and Engineering, 67056 Ludwigshafen, Germany

ARTICLE INFO

Article history:
Received 31 March 2011
Revised 18 May 2011
Accepted 19 May 2011
Available online 6 July 2011

Keywords:
Hydroconversion
Zeolites
Expanded materials
Layered materials
RUB-39

ABSTRACT

The layered silicate RUB-39 can be transformed by topotactic condensation into RUB-41 (RRO), a zeolite with 8- and 10- ring pores. If the layered RUB-39 is first silylated with dichlorodimethylsilane (DCDMS) or hexamethyldisiloxane (HMDS), an interlayer expanded structure is created after calcination. The DCDMS expanded material contains 10- and 12-ring pores instead of 8- and 10-ring pores. Detailed physicochemical characterization showed that the Al content is not significantly changed during the expansion. In the hydroconversion of decane, the expanded materials have a significantly increased activity, as demonstrated by the lower temperatures at which isomerization and cracking occur. Detailed comparison of the product selectivities obtained with RUB-41 or with its expanded analogs shows that the void structure of the expanded materials is significantly less constrained, as reflected in the distribution of methylnonane isomers, of the ethyloctane vs. methylnonane isomers, and in the ratio of monobranched vs. dibranched isomers.

1. Introduction

Zeolites are widely used as heterogeneous catalysts for the production of petrochemicals and fine chemicals. Because of the permanent quest for more sustainable processes and because of the ever more demanding requirements to the catalysts for these processes, there is a continued search for new zeolite materials with improved catalytic properties [1]. In an innovative approach to zeolite synthesis, layered silicates are prepared in a first step; upon calcination, these may transform by topotactic condensation into three-dimensional silicate frameworks. In some cases, the topotactic condensation of new layered materials results in well-known structures. For example, PREFER transforms upon calcination into ferrierite [2].

In other cases, the calcination of the layered precursor materials results in previously unknown structures. For instance, EU-19 [3], Nu-6 [4], PLS-1 [5], or RUB-18 [6] transform upon calcination into EU-20b, Nu-6(2), CDS-1, and RUB-24, with CAS, NSI, CDO, and RWR topologies, respectively. However, in all these materials, the pores are narrow and hardly accessible to reactants. In order to create more attractive materials for catalysis, the layered precursor can be treated after *synthesis* [7,8]. Delamination can be achieved via swelling of the lamellar precursor with a surfactant. For instance, full delamination of the precursor material MCM-22(P) resulted in the formation of ITQ-2 [9]. Alternatively, MCM-22(P) can be pillared by the use of a swelling agent and a treatment with tetraethylorthosilicate, resulting in a material named MCM-36 [10]. ITQ-2 and MCM-36 showed an improved access to the catalytic sites in the hydroconversion of *n*-decane compared with MCM-22 [11]. Recently, zeolite UTL was converted into a lamellar material with zeolite-like layers. This new material can be further modified in a similar way to other layered materials [12].

A new and versatile method of converting 2D lamellar precursors has been reported by the groups of Wu, Tatsumi, and coworkers [7,13]. They prepared Interlayer Expanded Zeolites (IEZ) by inserting monomeric Si compounds into the interlayer spaces via a one-step dialkoxysilylation followed by the removal of the organic moieties. IEZ materials were prepared starting from layered silicates PLS-1, MWW(P), PREFER, and MCM-47. Diethoxydimethylsilane (DEDMS) or dichlorodimethylsilane (DCDMS) was employed as silylating agents. The two methyl groups serve to avoid intermolecular condensation; if triethoxymethylsilane or tetraethoxysilane (TEOS) are used, condensation

* Corresponding author.
E-mail address: dirk.devos@biw.kuleuven.be (D.D. Vos).

0021-9517/$ - see front matter © 2011 Elsevier Inc. All rights reserved.
doi:10.1016/j.jcat.2011.05.022

of the silanes can occur and amorphous silica is deposited on the zeolite crystals.

A recent addition to the group of layered silicate precursors is RUB-39. Upon calcination, this material yields the zeolite RUB-41 with RRO topology [14,15]. RUB-41 contains a 2-dimensional pore system with intersecting 8- and 10-ring pores. From structure analysis, their dimensions are determined as 0.58×0.41 nm (8MR) and 0.59×0.41 nm (10MR). In previous work, we demonstrated the selective uptake of *trans*-2-butene and *cis*-2-butene from an isomeric butene mixture on the all silica RUB-41 [16]. This selectivity was ascribed to the distorted 10-ring present in RUB-41. In later work, Al was incorporated into this structure. (H)Al-RUB-41 was employed in the amination reaction of methanol with ammonia. (H)Al-RUB-41 showed a high selectivity (87%) toward monomethylamine and dimethylamine, a behavior which is typically expected for a small pore zeolite. This was attributed to the unique pore architecture of the material with its distorted 10 channels, which for this reaction seem spatially more restrictive than the 10-MR in, e.g., MFI or MEL zeolites [17].

Here, we report on materials obtained by interlayer silylation of the layered RUB-39 precursor material. After exposure of RUB-39 to dichlorodimethylsilane (DCDMS) or hexamethyldisiloxane (HMDS), followed by calcination, new expanded structures are formed. In this work, the catalytic effect of the interlayer expansion is investigated using the hydroconversion of decane as a test reaction. The composition of the branched isomerization products formed from decane is used to evaluate whether effectively the interlayer expansion results in a modified intracrystalline zeolite pore architecture.

2. Materials and methods

2.1. Catalyst preparation

Al-RUB-39 was synthesized by a 2-step synthesis procedure. First 0.215 mol NaOH was dissolved in 230 mL H_2O; then, 653.4 g of a 39 wt.% solution of dimethyldipropylammoniumhydroxide in H_2O was added, followed by 8.6 g RUB-39 seeds. After 10 min stirring, 208.5 g aerosil 200 was added. After aging of the gel for 1 h at room temperature, it was kept in a Teflon-lined stainless steel autoclave and stirred at a temperature of 140 °C at 15 rpm for 48 h. Hereafter, the mixture was cooled down and 5 g aluminumisopropoxide was added to the gel followed by crystallization at 150 °C for 48 h. Then, the obtained powder was filtered, washed with distilled water, and dried in an oven for 24 h at 120 °C. Part of the RUB-39 obtained was converted to Al-RUB-41 by slow heating at 1 °C per min until 520 °C in a furnace under static air. After 12 h at this temperature, heating was continued until 560 °C for 4 h. The other part of the synthesis product was used for the synthesis of an interlayer-expanded zeolite.

RUB-39/DCDMS and RUB-39/HMDS were synthesized by adding 36.2 g of a 1 M solution of HCl and 2 g RUB-39 in 84.1 g H_2O. After 10 min stirring, 0.4 g dichlorodimethylsilane (DCDMS) or 0.5 g hexamethyldisiloxane (HMDS) was added, and the suspension was transferred to an autoclave at 170 °C for 24 h. Then, the powder was washed, dried at 120 °C for 24 h, and calcined at 500 °C for 15 h with a temperature increase of 1 °C/min. To eliminate any Na^+ that could be present as a residue from the synthesis and to improve platinum dispersion, samples were three times ion-exchanged in a solution of 0.5 M NH_4NO_3 at 80 °C for 24 h and washed with distilled water. Next, these samples were dried at 70 °C. The bifunctional catalysts were prepared by impregnating 200 mg catalyst in 5 mL of a 0.001 M $Pt(NH_3)_4Cl_2$ aqueous solution for 24 h. They contained 0.5 wt.% of Pt on dry zeolite basis. The Si/Al ratio of the samples obtained was 50. Catalyst pellets with a size between 125 and 250 μm were obtained by pressing the powder, crushing into flakes, and sieving.

2.2. Characterization

X-ray powder diffraction analysis was carried out with a Siemens 5000D diffractometer using Cu Kα radiation ($\lambda = 0.15401$ nm). Nitrogen adsorption isotherms were determined by physisorption at 77 K on a Coulter Omnisorp 100 CX. Prior to measurements, the samples were outgassed under vacuum at 473 K overnight. SEM micrographs were recorded using a Philips XL30 FEG. ^{27}Al MAS NMR spectra of the samples were acquired on a Varian Infinity Plus-400 spectrometer at 104.2 MHz using a 4 mm MAS NMR probe head with a spinning rate of 10 kHz. Chemical shifts were referenced to $(NH_4)Al(SO_4)_2{\cdot}12H_2O$ at −0.4 ppm as a secondary reference. All spectra were accumulated for 12,000 scans with a $\pi/4$ flip angle and a 2 s pulse delay. Nitrogen adsorption isotherms were determined by physisorption of nitrogen at 77 K on a Coulter Omnisorp 100 CX. Prior to the measurements, the samples were outgassed under vacuum at 473 K overnight.

The temperature programmed desorption of ammonia (NH_3-TPD) experiments were carried out using a Micromeritics AutoChem II 2920 automated chemisorption analysis unit with a thermal conductivity detector (TCD) under helium flow. Samples were heated with a temperature ramp of 20 °C/min to 500 °C under He flow. After staying at that temperature for 10 min, they were cooled down to 100 °C in He atmosphere. Ammonia saturation was carried out at 100 °C using a 10% NH_3–He gas mixture. After saturation, excess ammonia was purged from the chamber under flowing He at 100 °C for 1 h. The desorption step was performed with a temperature ramp of 10 °C/min up to 500 °C under He flow. Desorbed species were observed with the online mass spectroscopy unit, which confirmed that the TCD signal indeed corresponded to ammonia desorption. The two peak intensities in the TPD traces were obtained via deconvolution.

2.3. Reaction conditions

The n-decane hydroconversion experiments were carried out at temperatures ranging from 140 till 300 °C, 4.5 bar H_2 pressure, a H_2/HC molar ratio of 375, and a space time of 2522 kg/s mol. Before reaction, the Pt-loaded NH_4^+ zeolite samples were first treated *in situ* in the flow reactor with an O_2-flow of 1.8 ml/min at 400 °C for the oxidation and then with a H_2-flow of 3.75 ml/min at 400 °C for the reduction of platinum. Intermediate cooling was performed in inert (helium) atmosphere.

From the exit of the vapor phase flow reactor, samples could be injected into a capillary GC equipped with a 25 m CPSil5 column, allowing separation of cracked products, n-decane and its monobranched products. The dibranched and tribranched decane isomers were lumped together. From the intensity of n-decane peak before and during reaction, actual conversions could be calculated (X). From the respective chromatograms, isomerization and cracking selectivity and product distributions in particular classes of products could be obtained.

3. Results

3.1. Characterization

The layered RUB-39 was synthesized following the recipe mentioned in the experimental section. When this precursor is calcined, it transforms by topotactic condensation into the RUB-41 zeolite with RRO topology [15]. The precursor can also be expanded with DCDMS and HMDS. The precursor that was used for

these expansions originates from the same synthesis batch as the RUB-41 zeolite and has a Si/Al ratio of 51. Fig. 1 shows SEM micrographs of the materials RUB-41, DCDMS, and HMDS expanded RUB-39.

In Fig. 1A, the typical platelet-like crystals of RUB-41 are shown. The crystal dimensions are about 5–20 μm in diameter and less than 1 μm in thickness. The SEM micrographs of the expanded RUB-39 materials (Fig. 1B and C) show similar crystal morphologies. The platelet-like morphology that is characteristic for RUB-41 is still observed. Comparison of the crystal dimensions shows that the crystals of the expanded materials have become somewhat smaller (1–5 μm). During the expansion treatment, some of the larger platelet-like precursors might have broken up into smaller fragments.

Fig. 2 shows the X-ray diffractograms of RUB-39, RUB-41, DCDMS expanded RUB-39 and HMDS expanded RUB-39. The untreated samples (a and b) show flat baselines, while the silylated samples (c and d) show a broad underlying maximum, pointing to the presence of less structured (amorphous-like) silica. The XRD pattern of the precursor has a characteristic diffraction at 8.12° 2θ, corresponding to an interlayer distance of 10.9 Å. Direct calcination leads to RUB-41 with a characteristic diffraction at 10.14° 2θ. As can be deduced from the shift of the first diffraction peak to higher angles, removal of the organic template and condensation of the interlayer hydroxyls upon calcination leads to a decrease in interlayer spacing to 8.7 Å. When the precursor is silylated, stable and crystalline materials were obtained even after calcination in air. These crystalline materials show a diffraction pattern that is different from that of RUB-41. Note that the characteristic diffractions at 11° and 13.5° are preserved for all samples; these are representative for intralayer ordering.

For the material silylated with DCDMS, a sharp diffraction is observed at 7.98° 2θ, showing that after the silylation, the interlayer distance (11.1 Å) is not very different from that in the layered precursor with the template still present. This proves that a silicon atom has been successfully inserted in between the layers, through displacement of the two –Cl groups via reaction with silanol groups from the layers above and below. A clearly different material is obtained by silylation using HMDS, in which each Si atom bears only one readily displaceable group. The first, somewhat broadened diffraction at 8.65° 2θ (10.2 Å interlayer distance), proves that the layers are on the average still significantly further apart than in the condensed RUB-41 material. The possibility that a pair of two Si atoms would be inserted in between the layers can be discarded based on the interlayer distance of only 10.2 Å, which is even smaller than for the material with insertion of a single Si atom (RUB-39/DCDMS).

In Fig. 3, the ^{27}Al MAS NMR spectrum of RUB-41, RUB-41 DCDMS, and RUB-41 HMDS is given. The signal at 54 ppm is assigned to framework tetrahedral aluminum (FAl) and the other one at about 0 ppm to octahedral extra-framework aluminum

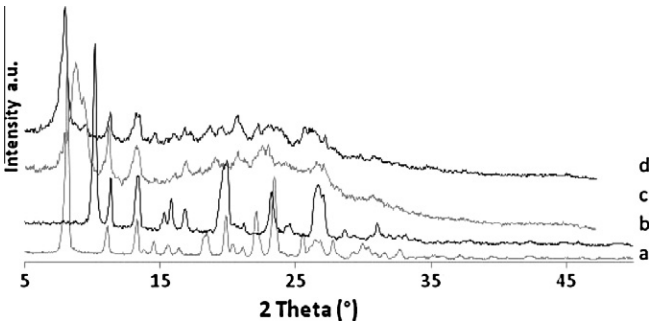

Fig. 2. XRD diffractograms of RUB-39 (a), RUB-41 (b), RUB-39 HMDS expanded (c), and RUB-39 DCDMS expanded (d).

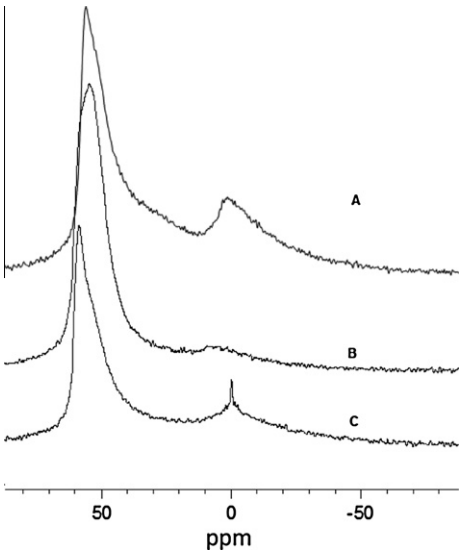

Fig. 3. ^{27}Al MAS NMR on (a) RUB-41, (b) RUB-39 DCDMS, and (c) RUB-39 HMDS.

(EFAl) in the samples [18]. The spectra indicate that the FAl resonance line is dominant in all samples.

In Table 1, the NH_3-TPD data of RUB-41, RUB-39/DCDMS, and RUB-39/HMDS are given. The first desorption maximum around 170 °C gives an indication of the amount of weakly interacting, physisorbed ammonia in the material. There is no clear indication that the silylation resulted in a change in the number of weak sites. Silylation also did not influence the number of strongly acidic sites as can be seen from the intensity of the second desorption maximum, corresponding to the thermal decomposition of ammonium ions. The expansion even seems to point to a small increase in acid strength as can be derived from the shift of the second peak to

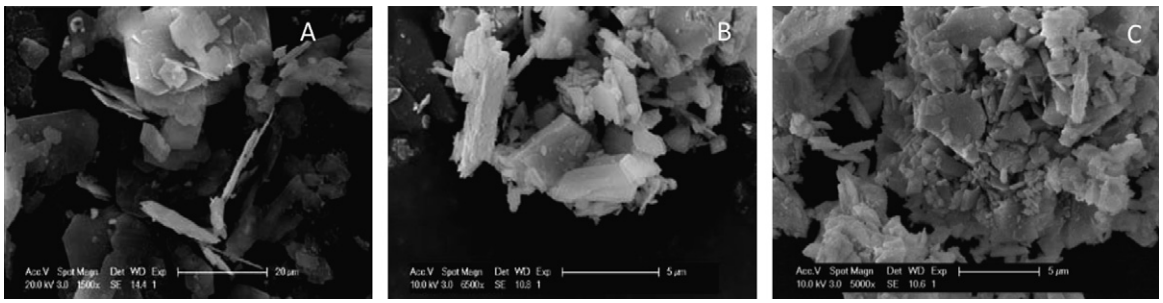

Fig. 1. SEM micrograph of RUB-41 (A), RUB-39 HMDS (B), and RUB-39 DCDMS (C).

Table 1
NH_3-TPD and N_2 adsorption data on RUB-41, RUB-39/HMDS, and RUB-39/DCDMS.

	NH_3-TPD[a]				Sorption properties	
	$T_{1,max}$ (°C)	Peak 1 (mmol g^{-1})	$T_{2,max}$ (°C)	Peak 2 (mmol g^{-1})	Langmuir/BET surface (m^2/g)	Micropore/mesopore volume (cm^3/g)
RUB-41	169	0.044	391	0.110	458/350	0.154/0.058
RUB-39/HMDS	176	0.046	437	0.121	364/278	0.120/0.054
RUB-39/DCDMS	171	0.047	428	0.109	431/328	0.137/0.086

[a] The subscripts 1 and 2 refer to the first and second NH_3 desorption peaks in Fig. 3.

higher temperatures. This can be the result of dilution of some existing FAl species after silylation.

The sorption properties of the samples are collected in Table 1. The sorptive properties of RUB-41, *viz.* specific surface and micropore volume, show reduced values upon silylation. While it may be expected that a stacking fault-free expansion will result in an increase in pore volume, for RUB-39/DCDMS, the small loss in micropore volume is fully compensated by an increase in the mesoporous volume. For RUB-39/HMDS, a slight decrease in the total porosity is observed. This can be ascribed to an imperfect silylation treatment, which could result in stacking faults or partial pore blocking.

3.2. n-Decane hydroconversion

In Fig. 4, the results of the hydroconversion of decane are given, in terms of temperature dependence of overall conversion, isomerization, and hydrocracking selectivity. The total conversion curves are shifted to lower temperatures for the silylated samples. At 210 °C, RUB-41 shows a conversion of 15.7%, whereas DCDMS and HMDS expanded RUB-39 show a conversion of 32.2% and 54.2%, respectively. As the amount of acid sites is essentially the same for the expanded materials as for the parent RUB-41, the higher activity could be related to the enhanced acid strength as already derived from the ammonia desorption measurements. As the characteristic steep slope of the curves, typical for hydroisomerization, is parallel in the three cases, it is unlikely that the presence of expanded pore windows in the silylated materials, resulting in a better diffusion of the reactants to the catalytic sites, or the slightly smaller crystal sizes, are at the basis of this difference.

In the expanded materials, the isomerization selectivity is also very significantly enhanced and typical for the consecutive nature of isomerization and hydrocracking in open pore H-zeolites loaded with Pt clusters. Among the other factors, a better distribution of the Pt inside the pores of the expanded materials may play an important role. Indeed, it is known that the 10-MR pores of RUB-41 are distorted, making the uptake of the Pt tetramine precursor more difficult. In *ideal* hydroconversion of n-alkanes, however, the hydrogenation/dehydrogenation on the metal phase should be significantly faster than the acid-catalyzed conversion C–C bond scission [19] and metal-catalyzed C–C hydrogenolysis as well as consecutive acid-catalyzed C–C cracking should be absent. The contribution of both reactions to ideal hydroisomerization should be reflected in the presence C_1,C_2 and C_8, C_9 fragments and in the asymmetry of the cracked product distribution among their carbon number. From Fig. 5, it follows that only traces of C_1, C_2, C_8, and C_9 are present at 5% hydrocracking, pointing to the absence of hydrogenolysis on metal sites, exerting exclusively their role in establishing a fast hydrogenation/dehydrogenation equilibrium among reactant and products. The almost symmetric distribution of the cracked products among their carbon number confirms the fast establishment of the hydrogenation/dehydrogenation equilibrium, stopping the C–C scissions after a single hydrocracking step. The more pronounced asymmetry in this distribution for the parent sample points to the occurrence of some secondary hydrocracking and thus to the existence of a minor unbalance of the activity between the two catalytic functions involved.

n-Decane hydroisomerization occurs via consecutive formation of mono-, di-, and multibranched isomers, with branchings centrally positioned in the hydrocarbon chain and thus characterized by increasing bulkiness. At the same moment, an increasing number of isomers with ααγ-configurations are formed, which are very susceptible to C–C scission. As a result of all this, the product selectivity in zeolite topologies with reduced pore sizes will be affected as follows:

- reduction of the isomerization maximum and
- reduction of the formation of C_5 fragments, stemming from centrally multibranched feed isomers.

This latter is more pronounced for the parent RUB-41 sample than for the silylated forms, showing a typical M-shaped pattern, commonly observed for H-ZSM-5. It points to the presence of reduced space for hydroconversion of n-decane in the former sample.

Fig. 6 confirms experimentally changes in behavior in the consecutive formation of monobranched and dibranched feed isomers. For the expanded samples, this occurs already starting at low isomerization conversion. For the parent sample, the selectivity for

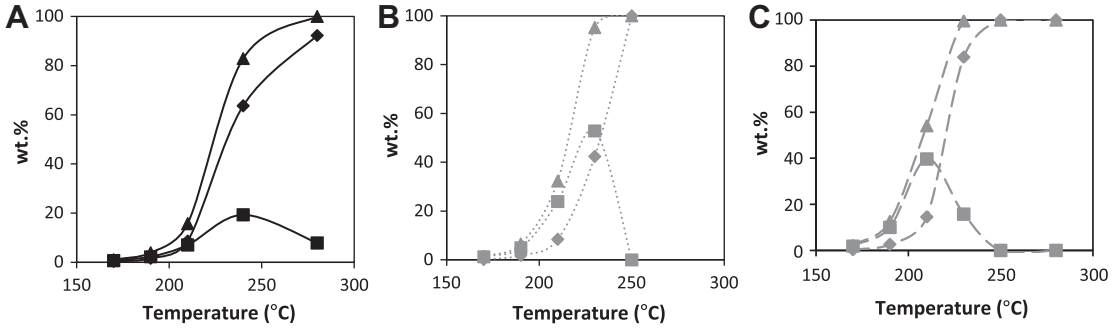

Fig. 4. Conversion of n-decane (▲) and selectivity for cracking (♦) and isomerization products (■) for RUB-41 (A), RUB-39/DCDMS (B) and RUB-39/HMDS (C) as a function of reaction temperature.

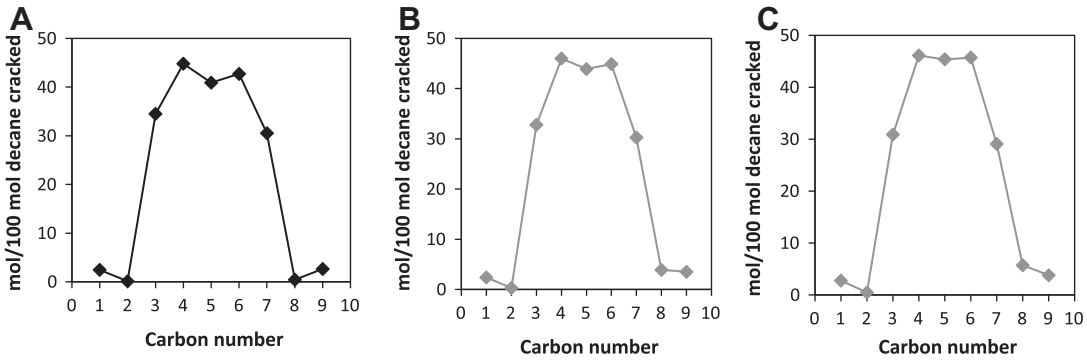

Fig. 5. Distribution of hydrocracked products at 5% cracking conversion: (A) RUB-41, (B) RUB-41 DCDMS, and (C) RUB-41 HMDS.

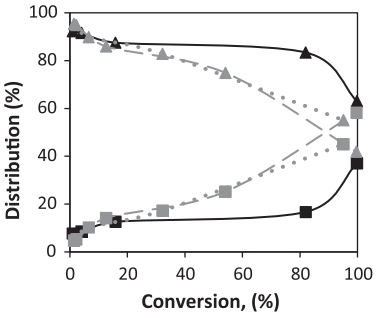

Fig. 6. Distribution of monobranched (▲) and dibranched (■) structures among the feed isomers in the hydroconversion of decane against conversion with RUB-41 (full line, black), RUB-39/DCDMS (dotted line, gray), and RUB-39/HMDS (hyphenated line, gray).

mono-branched isomers is high and constant up to high conversion, pointing to the lack of porosity needed for consecutive multibranching. At maximum isomerization conversion, the formation of monobranched isomers and dibranched isomers is in equilibrium; deviations of this equilibrium reflect the presence of steric constraints.

The expanded materials show a higher selectivity for dibranched isomers than the RUB-41 zeolite. Hence, less steric constraints are present, which can be explained by the increase in pore window size and the more spacious surroundings of the active sites.

In Fig. 7, the relative distribution of the individual methylnonanes is given against conversion. Methylbranching occurs via protonated cyclopropane (PCP) intermediates. If methylnonane formation from decane was statistical, one would obtain following distribution: 17%, 33%, 33%, and 17% for 2-MeC_9, 3-, 4-, and 5-MeC_9, respectively [20,21]. This is explained by the number of PCP intermediates formed from *n*-decane, assuming identical rates for their formation. In zeolites with small cavities and/or 10-ring (10-MR) pores, the formation of 2-MeC_9 is favored at the expense of especially 4- and 5-MeC_9. For RUB-41, the formation of 2-methylnonane is strongly enhanced. This behavior is typical for a 10-MR structure. For the expanded materials, the formation of 2-methylnonane is still enhanced but it is markedly lower than for RUB-41. This means that in the expanded materials, a constrained environment is still present, although it is somewhat more spacious than in a typical 10-MR zeolite. This can be rationalized based on the distorted 12-MR in this type of material.

The relative contribution of the ethyloctanes to the monobranched isomers is another criterium that gives an insight into the pore architecture of zeolites in general and of the interlayer expanded zeolite materials in particular (Fig. 8). Equilibration of the methylbranched isomers can occur via classical methyl- or alkyl-shifts. Methylnonanes are formed via protonated cyclopropanes, whereas ethyloctanes are formed via protonated cyclobutanes, the latter having a larger kinetic diameter than the PCPs. The formation of ethyloctanes and their diffusion out of the structure is sterically hindered in narrower pores. RUB-41 forms more methylnonanes compared with the expanded materials. RUB-39/DCDMS has a slightly higher ethyloctane formation. For HMDS expanded RUB-39, the difference is even more pronounced. The strongly enhanced ethyloctane formation over this material is indicative of wider pores compared with RUB-41.

3.2.1. Pore architecture estimation in reaction conditions

The n-decane hydroconversion via a series of product peculiarities has been used to relate product distributions with structural elements of known zeolite structures and thus to estimate the pore architecture of Pt-loaded zeolites in reaction conditions [20]. Interpolation of values in the respective relations obtained for known topologies even has allowed to describe the pore architecture of unknown zeolites. Indeed, the MCM-22 structure, in terms of pore

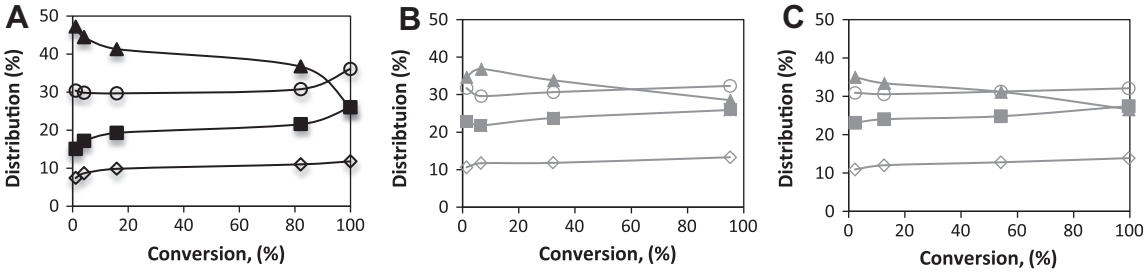

Fig. 7. Methylnonane distribution of RUB-41 (A), RUB-39/DCDMS (B), and RUB-39/HMDS (C) in function of conversion: (▲) 2-methylnonane, (○) 3-methylnonane, (■) 4-methylnonane, (◇) 5-methylnonane.

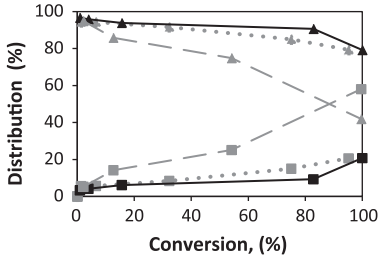

Fig. 8. Methylnonane (▲)/ethyloctane distribution (■) of RUB-41 (full line, black), RUB-39/DCDMS (dotted line, gray), RUB-39/HMDS (stripes, gray).

architecture, has been correctly predicted before determination of the structure via elaborate physical methods, indicative of the power of the method [22].

In Fig. 9, the distribution of monobranched and dibranched isomers at maximum isomerization conversion is given for a set of benchmark zeolite topologies [20]. The isomer distribution of the expanded materials is comparable with that obtained with 12-MR zeolites. The formation of dibranched isomers on RUB-39/HMDS is very high and comparable with that on 12-MR zeolites like mordenite. For RUB-39/DCDMS, the formation of dibranched isomers is even more pronounced and equals that of the monobranched ones; it approaches that obtained on open zeolite topologies like FAU and BEA. Somewhat unexpectedly, RUB-41 has a slightly enhanced formation of dibranched isomers compared to 10-zeolites with, e.g., MFI or MEL topology. This might result from the higher temperature at which maximum isomerization occurred. At this temperature, more isomerization could have occurred on weaker acid sites at the external surface.

In Fig. 10, the methylnonane and ethyloctane distributions at 5% isomerization conversion for a set of known zeolite structures are plotted against each other. Zeolites with 10-MR pores inhibit the formation of ethyloctanes in their void space. Straight 12-MR pores only allow minor quantities of ethyloctanes to be formed. Although for 12-MR zeolites with cages more ethyloctanes are formed, ethyloctane formation is still far from thermodynamic equilibrium (~17% ethyloctanes). The expanded materials have a higher ethyloctane formation compared with RUB-39 but are not as open as 12-MR zeolites containing cages or large pore intersections. RUB-41 has a high formation of ethyloctanes compared to other 10-MR zeolites. Possibly part of the isomerization happened on the external surface or as is the case for 8-MR zeolites, enough

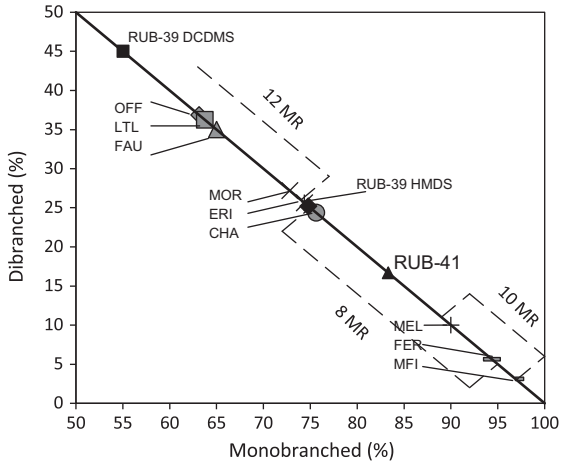

Fig. 9. Distribution of monobranched against dibranched feed isomers at maximum isomerization conversion with RUB-41 (▲), RUB-39/DCDMS (■), RUB-39/HMDS (♦), interpolated among zeolites with known topology [20].

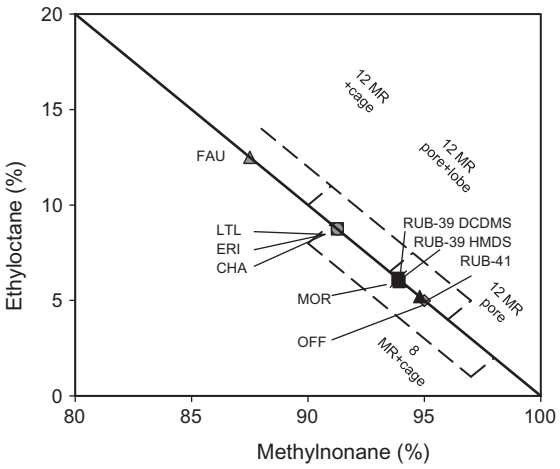

Fig. 10. Distribution of the sum of ethyloctanes against that of methylnonanes at 5% isomerization conversion with RUB-41 (▲), RUB-39/DCDMS (■), RUB-39/HMDS (♦), interpolated among zeolites with known topology [20].

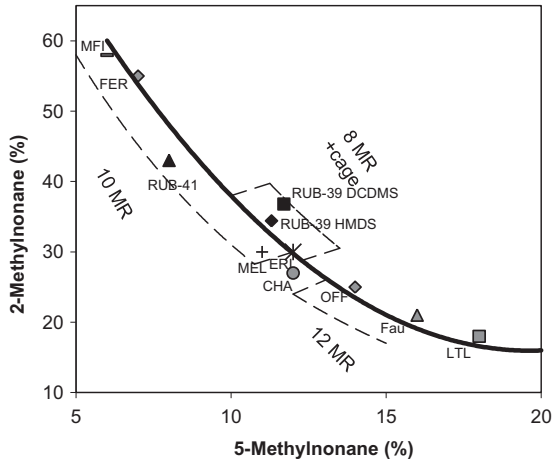

Fig. 11. Distribution of 2-methylnonane against 5-methylnonane at 5% isomerization conversion with RUB-41 (▲), RUB-39/DCDMS (■), RUB-39/HMDS (♦), interpolated among zeolites with known topology [18].

space is available in between the layers for the formation of ethyloctanes.

In Fig. 11, the relative distribution of 2-methylnonane against 5-methylnonane at 5% isomerization conversion is given for RUB-41, RUB-39/HMDS, and RUB-39/DCDMS. It is clear that due to transition state shape-selective effects, the rate of 2-methylnonane formation for RUB-41 is enhanced and located somewhere between that of MFI and MEL 10-MR zeolites. RUB-39/DCDMS and RUB-39/HMDS also have an enhanced 2-methylnonane formation compared with the statistical distribution, but the steric constraints are less pronounced than for RUB-41 and comparable to those of MEL zeolites.

4. Conclusion

Starting from the layered precursor RUB-39, different materials were synthesized. If RUB-39 is calcined, the 8- and 10-MR zeolite RUB-41 is obtained. If RUB-39 is silylated with HMDS or DCDMS, new materials are formed with expanded pore windows. In the hydroconversion of decane, it appears that RUB-41 largely shares

characteristics of 10-MR zeolites. Apparently, some of the criteria employed, like the ethyloctane formation, seem to indicate that RUB-41 is slightly more spacious than other 10-MR zeolites; however, this could be due to a contribution of the outer surface at the relatively elevated temperatures that were required for the isomerization. Note that RUB-41 has a very unusual pore architecture, with distorted 10-MR channels running through an interlayer gallery. The expanded materials show higher activity at lower temperatures compared to RUB-41, which in line with ammonia TPD and ^{27}Al MAS NMR measurements points to the generation of enhanced acid site strength. This is tentatively ascribed to the dilution of some of the lattice Al atoms by the silylation treatment. All shape selectivity criteria indicate that the structures are considerably more open than those of RUB-41 or other 10-MR zeolites. However, there seem to be more steric constraints than in typical 12-MR zeolites. This can be rationalized by the existence of distorted shape of the 12-MRs in an expanded material like RUB-39/DCDMS. In general, it is clearly proven that well-ordered catalytic materials, with high activity and controllable shape selectivity, are formed by the interlayer expansion strategy.

Acknowledgments

Support form BASF AG is acknowledged in the frame of an INCOE project. BT thanks IWT-Flanders for a fellowship.

Appendix A. Supplementary material

Supplementary data associated with this article can be found, in the online version, at doi:10.1016/j.jcat.2011.05.022.

References

[1] B. Yilmaz, U. Muller, Top Catal. 52 (2009) 888.
[2] L. Schreyeck, P. Caullet, J.C. Mougenel, J.L. Guth, B.J. Marler, Chem. Soc. – Chem. Commun. (1995) 2187.
[3] B. Marler, M.A. Camblor, H. Gies, Micropor. Mesopor. Mater. 90 (2006) 87.
[4] S. Zanardi, A. Alberti, G. Cruciani, A. Corma, V. Fornes, M. Brunelli, Angew. Chem. – Int. Edit. 43 (2004) 4933.
[5] T. Ikeda, Y. Akiyama, Y. Oumi, A. Kawai, F. Mizukami, Angew. Chem. – Int. Edit. 43 (2004) 4892.
[6] B. Marler, N. Stroter, H. Gies, Micropor. Mesopor. Mater. 83 (2005) 201.
[7] P. Wu, J.F. Ruan, L.L. Wang, L.L. Wu, Y. Wang, Y.M. Liu, W.B. Fan, M.Y. He, O. Terasaki, T.J. Tatsumi, Am. Chem. Soc. 130 (2008) 8178.
[8] W.J. Roth, J. Cejka, Catal. Sci. Technol. 1 (2011) 43.
[9] A. Corma, V. Fornes, S.B. Pergher, T.L.M. Maesen, J.G. Buglass, Nature 396 (1998) 353.
[10] W.J. Roth, C.T. Kresge, J.C. Vartuli, M.E. Leonowicz, A.S. Fung, S.B. McCullen, in: H.K. Beyer, H.G. Karge, I. Kiricsi, J.B. Nagy (Eds.), Catalysis by Microporous Materials, Elsevier Science Publisher BV, Amsterdam, 1995, p. 94: 301.
[11] S.B.C. Pergher, A. Corma, V. Fornes, Quim. Nova 26 (2003) 828.
[12] W.J. Roth, O.V. Shvets, M. Shamzhy, P. ChlubnaÃÅ, M. KubuÃä, P. Nachtigall, J. CÃåejka, J. Am. Chem. Soc. 133 (2011) 6130.
[13] S. Inagaki, H. Imai, S. Tsujiuchi, H. Yakushiji, T. Yokoi, T. Tatsumi, Micropor. Mesopor. Mater. 142 (2011) 354.
[14] Y.X. Wang, H. Gies, B. Marler, U. Muller, Chem. Mater. 17 (2005) 43.
[15] Y.X. Wang, H. Gies, J.H. Lin, Chem. Mater. 19 (2007) 4181.
[16] B. Tijsebaert, C. Varszegi, H. Gies, F.S. Xiao, X.H. Bao, T. Tatsumi, U. Muller, D. De Vos, Chem. Commun. (2008) 2480.
[17] B. Tijsebaert, B. Yilmaz, U. Muller, H. Gies, W.P. Zhang, X.H. Bao, F.S. Xiao, T. Tatsumi, D. De Vos, J. Catal. 278 (2011) 246.
[18] J.A. van Bokhoven, D.C. Koningsberger, P. Kunkeler, H.J. van Bekkum, J. Catal. 211 (2002) 540.
[19] H.L. Coonradt, W.E. Garwood, Ind. Eng. Chem. Process Des. Develop. 3 (1964) 38.
[20] J.A. Martens, M. Tielen, P.A. Jacobs, J. Weitkamp, Zeolites 4 (1984) 98.
[21] H. van Bekkum, E.M. Flanigen, J.C. Jansen (Eds.), Introduction to Zeolite Science and Practice, 1991, pp. 58.
[22] W. Souverijns, W. Verrelst, G. Vanbutsele, J.A. Martens, P.A.J. Jacobs, Chem. Soc. – Chem. Commun. (1994) 1671.